THE AMERICAN SOCIETY OF MECHANICAL ENGINEERS
345 E. 47 St., New York, N.Y. 10017

86-GT-190

Inverse Design of Composite Turbine Blade Circular Coolant Flow Passages

TING-LUNG CHIANG
Graduate Assistant

GEORGE S. DULIKRAVICH
Assistant Professor

Department of Aerospace Engineering
and Engineering Mechanics
The University of Texas at Austin, Austin, Texas

ABSTRACT

An inverse design and optimization method is developed to determine the proper size and location of the circular shaped holes (coolant flow passages) in a composite turbine blade. The temperature distributions specified on the outer blade surface and on the surfaces of the inner holes can be prescribed a priori. In addition, heat flux distribution on the outer blade surface can be prescribed and iteratively enforced using optimization procedures. The prescribed heat flux distribution on the outer surface is iteratively approached by using the Sequential Unconstrained Minimization Technique (SUMT) to adjust the sizes and locations of the initially guessed circular holes. During each optimization iteration, a two-dimensional heat conduction equation is solved using direct Boundary Element Method (BEM) with linear temperature singularity distribution. For manufacturing purposes the additional constraints are enforced assuring the minimal prescribed blade wall thickness and spacing between the walls of two neighboring holes. The method is applicable to both single material (homogeneous) and coated (composite) turbine blades. Three different cases were tested to prove the feasibility and the accuracy of the method.

INTRODUCTION

The idea of using optimization technique coupled with the panel method (a kind of indirect BEM, often used in fluid mechanics to solve Laplace's equation) to develop an inverse design method for multi-holed internally cooled turbine blades was originated by Kennon and Dulikravich [1,2,3,4]. They used panel method to solve Laplace's equation for the temperature field in the solid blade material subject to partly Cauchy type boundary conditions. The computed temperature distribution on the initially guessed inner coolant flow passage walls, and the prescribed coolant temperature on these walls were then iteratively approached by changing the shapes and sizes of the coolant flow passages until the procedure converged.

The present work represents an improvement over this method which can be summarized as follows

Presented at the International Gas Turbine Conference and Exhibit
Dusseldorf, West Germany—June 8-12, 1986

The temperature and heat flux distributions on the Γ_1 surface (Fig. 1) of the turbine blade are specified a priori in the original method. This is now changed to the temperature distribution and heat flux distribution specified on Γ_1 and the temperature distribution specified on Γ_3 surface, thus changing boundary conditions for the Laplace's equation from a partly Cauchy type to a Dirichlet type during each iterative step.

The objective function is changed to the error function defined by the differences between the calculated and specified heat flux distributions on the surface Γ_1 instead of differences in temperatures on the surface Γ_3.

The direct BEM is used presently instead of the panel method to solve the two-dimensional Laplace's equation for the steady state temperature field. Also, the elements used now have linear temperature distribution instead of the constant temperature distribution.

Two constraints that might be required in the practical blade manufacturing process are added. They allow a minimum distance d_0 to be maintained between any hole and the Γ_2 surface and a minimum distance d_i to be maintained between the walls of any two neighboring holes (Fig. 1).

The non-homogeneous blade design is allowed whereby a surface layer of, for example, ceramic material is used to coat the turbine surface Γ_2 (Fig. 1). This results in two coupled Laplace's equations that need to be solved simultaneously.

All the inner coolant flow passage shapes are forced to be circular, since the circular shape is more acceptable than the arbitrary shape from the manufacturing point of view.

ANALYTIC FORMULATION

There are two methods of formulating the boundary-value problems of potential theory. The first method is refered to as an indirect formulation. It represents the potential function, u, with a single-layer or a double-layer potential generated by continuous source distribution over a surface Γ. This procedure leads to the formulation of integral equations which define the source densities. This method is mainly used in fluid mechanics where it is known as the source panel method.

However, one of the disadvantages of the indirect formulation is that the calculated source strengths usually have no obvious physical relation to the problem [5]. The other disadvantage is that the boundary surface is restricted to be a Liapunov (smooth) one. These disadvantages can be overcome by using the direct formulation of the BEM [5].

The direct formulation can be deduced [5] from Green's third identity or the weighted residual method, since the latter permits a straightforward extension to solve more complex partial differential equations and can combine the BEM with more classical numerical methods. Therefore the latter method is usually used to formulate integral equations. The weighted residual statement can be written as :

$$\int_{\Omega} (\nabla^2 u) u^* \, d\Omega = \int_{\Gamma_N} (q-\bar{q}) u^* d\Gamma - \int_{\Gamma_E} (u-\bar{u}) q^* \, d\Gamma \qquad (1)$$

where u^* is the fundamental solution of the Laplace's equation on a domain Ω, that is,

$$\nabla^2 u^* + \Delta_i = 0 \qquad (2)$$

where Δ_i is the Dirac's delta function. For an isotropic two-dimensional medium,

$$u^* = \frac{1}{2\pi} \ln \frac{1}{r} \qquad (3)$$

where r is the distance from point i to the point under consideration.

Then

$$q = \frac{\partial u}{\partial n} \qquad q^* = \frac{\partial u^*}{\partial n} \qquad (4)$$

Usually, $u = \bar{u}$ on Γ_E are called the essential conditions and $\frac{\partial u}{\partial n} = \bar{q}$ on Γ_N are called the natural conditions.

Integrating by parts and substituting Eq. (2) into the left-hand side of Eq. (1), the final form of the boundary integral equation is :

$$c_i u_i + \int_\Gamma uq^* \, d\Gamma = \int_\Gamma qu^* \, d\Gamma \tag{5}$$

This equation provides a functional constraint between u and q over Γ, which ensures their compatibility as boundary data. Here, c_i is the value of the scaled internal angle of the boundary Γ at the point i (Fig. 2a), that is,

$$c_i = \frac{\theta}{2\pi} \tag{6}$$

Consequently, $c_i = 1/2$ for a point on a smooth boundary where there is a continuous tangent, $c_i = 1$ for a point in the interior Ω, and $c_i = 0$ for a point exterior to Ω.

NUMERICAL DISCRETIZATION

Equation (5) can be discretized into a series of straight elements on the surface Γ with the variation of u and q assumed to be linear along each element. The points where the unknown derivatives q of the potential are considered are called nodes and are taken to be at the ends of each element (Fig. 2a).

Equation (5) can be written for the n elements as :

$$c_i u_i + \sum_{j=1}^{n} \int_{\Gamma_j} uq^* \, d\Gamma = \sum_{j=1}^{n} \int_{\Gamma_j} qu^* \, d\Gamma \tag{7}$$

The values of u and q at any point of the element can be defined in terms of their nodal values and the linear interpolation functions ϕ_1 and ϕ_2, that is,

$$u(\xi) = [\phi_1 \phi_2] \begin{bmatrix} u_1 \\ u_2 \end{bmatrix} \tag{8}$$

$$q(\xi) = [\phi_1 \phi_2] \begin{bmatrix} q_1 \\ q_2 \end{bmatrix} \tag{9}$$

where ξ is the dimensionless coordinate (Fig. 2b), $\xi = 2x/l$

and $\phi_1 = \frac{1}{2}(1-\xi)$ $\phi_2 = \frac{1}{2}(1+\xi)$

Then

$$\int_{\Gamma_j} uq^* \, d\Gamma = [h^1_{ij} \, , \, h^2_{ij}] \begin{bmatrix} u_1 \\ u_2 \end{bmatrix} \tag{10}$$

where

$$h^1_{ij} = \int_{\Gamma_j} \phi_1 q^* \, d\Gamma \quad h^2_{ij} = \int_{\Gamma_j} \phi_2 q^* \, d\Gamma$$

Hence

$$\int_{\Gamma_j} qu^* \, d\Gamma = [g^1_{ij} \, , \, g^2_{ij}] \begin{bmatrix} q_1 \\ q_2 \end{bmatrix} \tag{11}$$

where

$$g^1_{ij} = \int_{\Gamma_j} \phi_1 u^* \, d\Gamma \quad g^2_{ij} = \int_{\Gamma_j} \phi_2 u^* \, d\Gamma$$

All coefficients h^1_{ij}, h^2_{ij}, g^1_{ij}, and g^2_{ij} can be evaluated by using the numerical integration. When i=j, g^1_{ij} and g^2_{ij} are determined analytically [5].

Substituting these into Eq.(7), the equation for node i can be obtained as

$$c_i u_i + [\hat{H}_{i1}, \ldots \hat{H}_{iN}] \begin{bmatrix} u_1 \\ \cdot \\ \cdot \\ \cdot \\ \cdot \\ u_N \end{bmatrix} = [G_{i1}, G_{i2}, \ldots G_{iN}] \begin{bmatrix} q_1 \\ \cdot \\ \cdot \\ \cdot \\ \cdot \\ q_N \end{bmatrix} \tag{12}$$

where for all $j \neq 1$

$$\hat{H}_{ij} = h^2_{i,j-1} + h^1_{i,j} \, , \quad G_{ij} = g^2_{i,j-1} + g^1_{i,j} \tag{13}$$

and for $j = 1$

$$\hat{H}_{i,j} = h^1_{i,1} + h^2_{i,N} \, , \quad G_{ij} = g^1_{i,1} + g^2_{i,N} \tag{14}$$

Then

$$c_i u_i + \sum_{j=1}^{N} \hat{H}_{ij} u_j = \sum_{j=1}^{N} G_{ij} q_j \tag{15}$$

or more simply

$$\sum_{j=1}^{N} H_{ij}u_j = \sum_{j=1}^{N} G_{i,j}q_j \qquad (16)$$

where

$$\begin{aligned} H_{i,j} &= \hat{H}_{i,j} \quad \text{for} \quad i \neq j \\ H_{i,j} &= \hat{H}_{i,j} + c_i \quad \text{for} \quad i = j \end{aligned} \qquad (17)$$

COMPOSITE BLADES

Turbine blades with, say, ceramic coating have two regions of considerably different thermal conductivities. Therefore, two coupled Laplace's equations for temperature field need to be solved. The corresponding two matrices can be added together by using the continuity of heat fluxes and equalizing the temperatures themselves at the interface Γ_2 between the coating and the main turbine material.

Assume that there are N_i elements on the surfaces Γ_i where i=1,2,3 and that the thermal conductivity in Ω_A is k_1 and in Ω_B is k_2. For domain Ω_A (coating material) the governing equations are then :

$$\underbrace{\begin{bmatrix} H_{1,1} & \cdots & H_{1,N_1} \\ \vdots & & \vdots \\ H_{N_1+N_2,1} & \cdots & H_{N_1+N_2,N_1} \end{bmatrix}}_{H_1^{\Omega_A}} \underbrace{\begin{bmatrix} H_{1,N_1+1} & \cdots & H_{1,N_1+N_2} \\ \vdots & & \vdots \\ H_{N_1+N_2,N_1+1} & \cdots & H_{N_1+N_2,N_1+N_2} \end{bmatrix}}_{H_2^{\Omega_A}} \begin{bmatrix} \Gamma_1 \\ u_1 \\ \vdots \\ \Gamma_1 \\ u_{N_1} \\ \Gamma_2 \\ u_1 \\ \vdots \\ \Gamma_2 \\ u_{N_2} \end{bmatrix} =$$

$$\underbrace{\begin{bmatrix} G_{1,1} & \cdots & G_{1,N_1} \\ \vdots & & \vdots \\ G_{N_1+N_2,1} & \cdots & G_{N_1+N_2,N_1} \end{bmatrix}}_{G_1^{\Omega_A}} \underbrace{\begin{bmatrix} G_{1,N_1+1} & \cdots & G_{1,N_1+N_2} \\ \vdots & & \vdots \\ G_{N_1+N_2,N_1+1} & \cdots & G_{N_1+N_2,N_1+N_2} \end{bmatrix}}_{G_1^{\Omega_A}} \begin{bmatrix} \Gamma_1 \\ Q_1/k_1 \\ \vdots \\ \Gamma_1 \\ Q_{N_1}/k_1 \\ \Gamma_2 \\ Q_1/k_1 \\ \vdots \\ \Gamma_2 \\ Q_{N_2}/k_1 \end{bmatrix} \qquad (18)$$

or more simply

$$\begin{bmatrix} \Omega_A & \Omega_A \\ H_1 & , H_2 \end{bmatrix} \begin{bmatrix} \Gamma_1 \\ u \\ \Gamma_2 \\ u \end{bmatrix} = \begin{bmatrix} \Omega_A & \Omega_A \\ G_1 & , G_2 \end{bmatrix} \begin{bmatrix} \Gamma_1 \\ Q \ /k_1 \\ \Gamma_2 \\ Q \ /k_1 \end{bmatrix} \qquad (19)$$

In the same way, for domain Ω_B (main blade material) :

$$\begin{bmatrix} \Omega_B & \Omega_B \\ H_1 & , H_2 \end{bmatrix} \begin{bmatrix} \Gamma_2 \\ u \\ \Gamma_3 \\ u \end{bmatrix} = \begin{bmatrix} \Omega_B & \Omega_B \\ G_1 & , G_2 \end{bmatrix} \begin{bmatrix} \Gamma_2 \\ -Q \ /k_2 \\ \Gamma_3 \\ Q \ /k_2 \end{bmatrix} \qquad (20)$$

Combining Eq.(19) and Eq.(20) and moving all the unknowns to the right-hand side results in

$$\begin{bmatrix} \Omega_A & & \\ k_1H_1 & 0 & \\ & \Omega_B & \\ 0 & k_2H_2 & \end{bmatrix} \begin{bmatrix} \Gamma_1 \\ u \\ \Gamma_3 \\ u \end{bmatrix} = \begin{bmatrix} \Omega_A & \Omega_A & \Omega_A & \\ G_1 & G_2 & -k_1H_2 & 0 \\ & \Omega_B & \Omega_B & \Omega_B \\ 0 & -G_1 & -k_2H_1 & G_2 \end{bmatrix} \begin{bmatrix} \Gamma_1 \\ Q \\ \Gamma_2 \\ Q \\ \Gamma_2 \\ u \\ \Gamma_3 \\ Q \end{bmatrix} \qquad (21)$$

Notice the directions of the normal defined on different surfaces as shown in Fig. 1. So, for surfaces Γ_1 and Γ_2, the numbering scheme is defined in the counterclockwise direction, while for Γ_3 it is in the clockwise direction.

PROBLEM OF THE NON-UNIQUENESS

For a multiply-connected domain, the solution of the integral equation with Dirichlet or mixed type boundary conditions does not always have a unique solution [6]. That is, for a given curve-shape Γ_1 there will always exist a particular curve-magnitude, where difficulties will occur in connection with the integral equations of the first kind with logarithmic kernel.

In the present work, this situation is avoided by a simple change of scale - a method adopted by Symm [6], so that the maximum diameter of the do-

main is not greater than unity. This is sufficient to ensure that there is no possibility of non-uniqueness due to Γ_1 being a Γ-contour. Alternatively, a unique solution may also be obtained by adding an appropriate auxiliary condition [7]. Detailed discussions on the non-uniqueness of the solutions of the integral equations can be found in [8] and [9].

THE OPTIMIZATION PROCEDURES AND CONCEPT

The iterative optimization procedure used to modify the sizes and locations of the quessed coolant flow passages can be explained using the following steps :

(1) Specify the potential (temperature) distributions u on surfaces Γ_1 and Γ_3.

(2) Specify the heat flux distribution Q^R_j (for $j=1,\ldots,N_1$) on surface Γ_1, and the thermal conductivities k_1 and k_2.

(3) Specify the manufacturing constraints (i) minimum distance d_0 allowed between the holes and surface Γ_2. (ii) minimum distance d_i allowed between any two neighboring hole surfaces Γ_3.

(4) Specify the number of holes required, and the initial guess of the radii and location of the centers of the holes. Also, required is specification of the number of boundary elements to be used on surfaces Γ_1, Γ_2, and each of the holes, Γ_3.

The geometry for each circular hole can be defined by three independent variables : center's coordinates x and y, and the radius r. So if there are M holes, there will be 3M independent variables in the error function.

However, the initially guessed variables should locate the holes entirely in the feasible region of domain Ω_B, that is, the constraints in step (3) must be satisfied (Fig. 1).

(5) With the BEM described earlier, solve Laplace's equation for temperature field and calculate the heat flux Q^C_j ($j=1,\ldots N_1$) on surface Γ_1.

(6) Use the Q^C_j to determine the values of the error function and the objective function (OBJ) of the optimization problem.

The non-dimensional error function E_0 can be defined as

$$E_o(\underset{\sim}{x}) = E_o(x_i,y_i;r_i) = \frac{\left[\sum_{j=1}^{N_1} (Q^C_j - Q^R_j)^2\right]^{1/2}}{\left[\sum_{j=1}^{N_1} (Q^R_j)^2\right]^{1/2}} \qquad (22)$$

The purpose is to find optimal value of $\underset{\sim}{x}(x_i,y_i;r_i)$ for i=1,...M such that E_0 is minimized. A penalty function must be added to E_o to construct the OBJ function $E^*(\underset{\sim}{x})$ for the two manufacturing constraints, that is,

$$E^*(\underset{\sim}{x}) = E_o(\underset{\sim}{x}) + \text{penalty function} \qquad (23)$$

There are many different forms for the penalty function [10]. The penalty function used here is of the interior method type with the inverse barrier function proposed by Carroll [11].

$$\text{Penalty function} = R\cdot\left[\sum_{j=1}^{N_3} \frac{d_o}{(D_j-d_o)} + \sum_{k=1}^{N_4} \frac{d_i}{(D_k-d_i)}\right] \qquad (24)$$

where $N_4 = \frac{N_3!}{2!(N_3-2)!}$ Here, D_j is the minimum computed distance between the element j of Γ_3 and the surface Γ_2 and D_k is the computed distance between any two circular holes.

$D_k = [(x_i-x_{i+1})^2 + (y_i-y_{i+1})^2]^{1/2} - (r_i + r_{i+1})$

for holes i and i+1.

R is a positive constant which is chosen to be initially quite large during the first few optimization iterations, and then gradually reduced to near zero $E^*(\underset{\sim}{x})$ will then approach E_0. This method is called the Squential Unconstrained Minization Techanique (SUMT).

A relation between the initial penalty func-

tion and the error function is defined as Penalty Adjustment Coefficient (P.A.Coeff), that is,

$$\text{P.A. Coeff} = \frac{\text{Penalty function}}{E_o}$$

(7) Use the steepest-descent optimization technique to find the new values of the indepent variables $\underset{\sim}{x}$ until the corresponding $E^*(\underset{\sim}{x})$ is below a satisfactory value, otherwise return to step (5).

RESULTS AND DISCUSSIONS

On the basis of preceeding analysis a computer program [12] was developed and tested using the following three test cases.

The first test case was used to test the reliability of the computer program as an analysis tool. The geometry consists of a coating and a single hole (Fig. 3) with $r_3:r_2\ r_1 = 0.5:0.8:1.2$, $k_1=1$, $k_2=5$, $T_1=100$, $T_3=20$ (uniform distributed). A total of 72 boundary elements were used. The results are listed in Table. 1, showing that the largest error between the analytic solution and the BEM solution is about 1.63% in Q_1. The accuracy of the BEM can be further improved by either increasing the number of elements or using higher order elements. The inverse optimization solutions were accomplished (Table 1) by specifying the heat flux distribution on Γ_1 and temperature distribution on Γ_1 and Γ_3 surfaces. The heat flux on Γ_1 surface was then calculated by the BEM after each iteration, that is, after each adjustment of the hole shapes and their locations. The initially guessed surface Γ_3 and its iterative evolution sequence are shown in Fig. 4.

The second test case was used to test the feasiblity of the inverse design concept. The same heat flux distribution on the surface Γ_1 was kept as in the first case, but the number of the circular holes was changed to three instead of one (Fig. 5a). Temperature distributions on Γ_1 and the holes Γ_3 did not change, that is, it was still $T_1=100$ on Γ_1 and $T_3=20$ on Γ_3. Comparsion of the calculated heat flux distribution with the specified heat flux is shown in Fig. 6. The corresponding L2-norm error was below 2% and it is distributed in the form of a sine function (see Fig. 6). It can be concluded that the inverse design concept is quite feasible for multihole configurations. Note that when the error was decreased to 0.829% (Fig. 5b), one of the three holes converged to a large hole located near the center. The other two holes became negligibly small in comparison with the large hole (Fig. 5b).

The third test case was used to prove that for an arbitrarily shaped blade, a good accuracy can be obtained between the BEM approximate solutions and the inverse optimization solutions.

The contour Γ_1 used in this case was a realistic turbine blade (Fig. 8). The variable temperature distribution specified on the surface Γ_1 can be seen in Fig. 7 and does not represent any actually measured value. The results of the inverse design procedure are listed in Table. 2 and the evolution history of the holes can be seen in Fig. 8.

No obvious irregularity can be seen from the convergence history of E_0 except when the P.A.Coeff. is chosen to be too big. Then, there will be an upshoot during the first iteration (see Fig. 9 and Fig. 10). Note that in Fig. 9 for the P.A.Coeff. equal to 8 and in Fig. 10 for the P.A.Coeff. equal to 0.5, the iterative process converged to local minimas.

Also, in the third test case using P.A.Coeff. of 10, resulted in an infeasible solution, that is, the radius of one of the circular holes became negative. Conclusion is that too big a P.A.Coeff. will create a large $E^*(\underset{\sim}{x})$ value, so the hole radius derived from the quadratic interploation will fall below a physically meaningful value. Conclusion is that P.A.Coeff. should be of the order one.

The rate of convergence of any optimum search technique is highly dependent on the given function E^* In certain problems a proper scaling can be performed so as to make the contours of constant error be as circular as possible. This can significantly accelerate the rate of convergence. Unfortunately, the $E^*(\underset{\sim}{x})$ in this inverse design problem is an implicit function of $\underset{\sim}{x}$ and the scaling technique is hard to apply.

The problem of failing to find the global minimum might be resolved in any optimization technique by recomputing the problem with different initial guesses [13]. The initial variables should be systematically chosen for good distribution over the variable space until a sufficiently low value of E_0 has been located.

SUMMARY

An efficient inverse design procedure for multiple circular holes(coolant flow passages) in non-homogeneous turbine blades has been developed. The work is accomplished by coupling the direct boundary element method and the sequential unconstrained minimization technique.

The specified heat flux distribution on the outer surface of the blade is iteratively approached while satisfying the prescribed temperature distributions on the outer surface of the blade and on surfaces of the holes by a successive adjument of the sizes and locations of the holes. Also included are two manufacturing constraints concerning the minimal allowable blade wall thickness and hole spacing.

This procedure can successfully be applied to the inverse design of coated turbine blade multiple coolant flow passage shapes. In earlier works [1,2,3,4] was demonstrated that the coolant flow passage shapes can be changed from circular to other families of non-circular holes by adjusting the relation between the independent variables in the optimization objective function. It can also be revised to be used for the inverse design and analysis of the transient thermal problems or coupled with forced convection boundary conditions on the coolant flow passage walls if the coolant temperature and heat transfer coefficients are provided.

REFERENCES

1. Kennon, S. R.,"Novel Approaches to Grid Generation, Inverse Design , and Acceleration of Iterative Schemes," M.S. Thesis, Dept. of Aerospace Eng. and Eng. Mechanics, University of Texas at Austin, May 1984.

2. Kennon, S. R. and Dulikravich, G. S., "The Inverse Design of Internally Cooled Turbine Blades," ASME Paper 84-GT-7, presented at 29th International Gas Turbine Conference, Amsterdam, The Netherlands, June 4-7, 1984.

3. Kennon, S. R. and Dulikravich, G. S., "Inverse Design of Multiholed Internally Cooled Turbine Blades," Proceedings of the International Conference on Inverse Design in Engineering Sciences (ICIDES), pp. 217-240, G. S. Dulikravich ed., University of Texas at Austin, October 17-18, 1984.

4. Kennon, S. R. and Dulikravich, G. S., "Inverse Design of Coolant Flow Passage Shapes with Partially Fixed Internal Geometries," ASME Paper 85-GT-118, presented at the 30th ASME International Gas Turbine Conference, Houston, Texas, March 17-21, 1985.

5. Brebbia, C. A., et al., "Boundary Element Techniques", Springer-Verlag, Berlin, Heidelberg, 1984.

6. Symm, G. T. "The Robin Problem in a Multiply-Connected Domain", in Boundary Element Methods in Engineering Proceedings of the Fourth International Seminar, Southampton, England, September, 1982.

7. Christiansen, S., "Integral Equations without a Unique Solution can be made Useful for Solving some Plane Harmonic Problems," J. Inst. Math. Applics., 16: pp. 143-159, 1975.

8. Jaswon, M. A., "Integral Equation Methods in Potential Theory," I. Proc. Roy. Soc. (A), 275: pp. 23-32, 1963.

9. Hayes, J. and Kellner, R., "The Eignvalue Problem for a Pair of Coupled Integral Equations Arising in the Numerical Solution of Laplace's Equation," SIAM J. Appl. Math., 22, 3: pp. 503-513, 1972.

10. Vanderpleats, G. N., "Numerical Optimization Techniques for Engineering Design : with Applications," McGraw-Hill, 1984.

11. Carroll, C. W., "An Operations Research Approach to the Economic Optimization of a Kraft

Pulping Process," Ph. D. Thesis, Institute of Paper Chemistry, Appleton, Wisconsin, 1959.

12. Chiang, T. L. and Dulikravich, G. S., "CFD8503- FORTRAN Program for Inverse Design of Coolant Flow Passages in Composite Turbine Blades," Computational Fluid Dynamics UTCFD Report 200-85, Dept. of Aerospace Eng. and Eng. Mechanics, University of Texas at Austin, September 1985.

13. Daniels, R. W.."An Introduction to Numerical Methods and Optimization Techniques," Elsevier North-Holland, New York, 1978.

Surface		Γ_1	Γ_2		Γ_3			
Properties / Method		Q_1	Q_2	T_2	Q_3	hole Center		hole Radius
						x	y	r
Analytic Solution		133.47	-200.21	35.06	-320.34	0.00*	0.00*	0.5*
BEM Approximate Solution		135.65	-200.43	35.21	-324.1	0.00*	0.00*	0.5*
Inverse Optimization Solution	P.A. Coeff							
	0.1	135.65*	-200.52	35.24	-324.74	0.00032	0.0006	0.4998
	1.0	135.65*	-200.44	35.21	-324.64	0.0001	0.0000	0.5001
	5.0	135.65*	-200.34	35.25	-324.90	0.0005	0.0003	0.4994

Table. 1 Results for the first test case : using linear BEM

* - values are given as the specified conditions

		Total Heat Flux on Surface			Hole 1			Hole 2			L2 Norm Error x 100%
					Center		Radius	Center		Radius	
		Γ_1	Γ_2	Γ_3	x_1	y_1	r_1	x_2	y_2	r_2	
Approximate Solution		70554	-70636	-71501	0.3*	1.25*	0.08*	0.5*	1.0*	0.05*	
Inverse Optimization Solution	P.A. Coeff										
	0.1	70570	-70653	-71648	0.2978	1.2511	0.0783	0.5031	1.008	0.053	0.927
	0.5	70214	-70298	-71339	0.2953	1.2530	0.0774	0.4997	1.021	0.055	2.346
	1.0	7.0564	-70647	-71648	0.2976	1.2512	0.0782	0.5031	1.009	0.054	0.991
	1.5	70556	-70639	-71635	0.2977	1.2512	0.0783	0.5031	1.008	0.054	0.95
	5.0	70564	-70647	-71646	0.2977	1.2512	0.0782	0.5031	1.008	0.054	0.972
	8.0	70585	-70669	-71664	0.2977	1.2512	0.0783	0.5031	1.008	0.053	0.921

Table. 2 Results for the third test case using linear element

* - values are given as the specified conditions

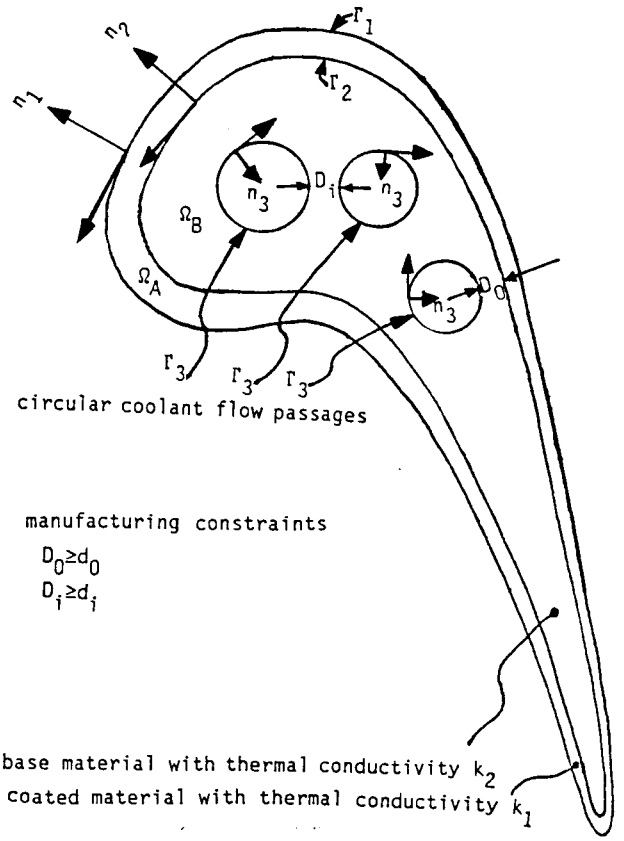

Fig. 1 Geometry and manufacturing constraints

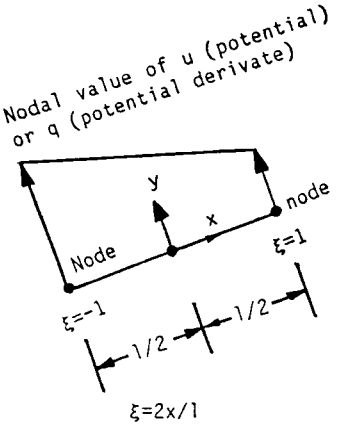

Fig. 2b Linear element

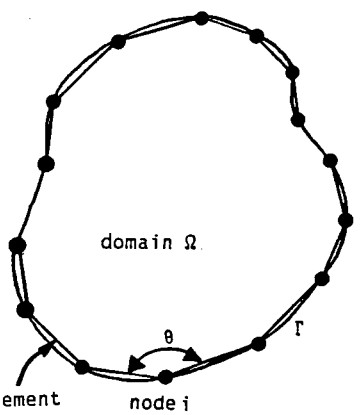

Fig. 2a Discretized boundary Γ

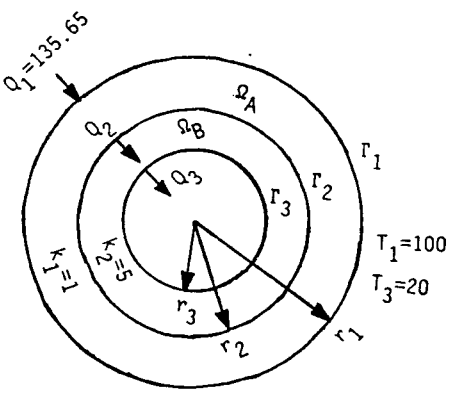

Fig. 3 Geometry and boundary conditions, test case 1

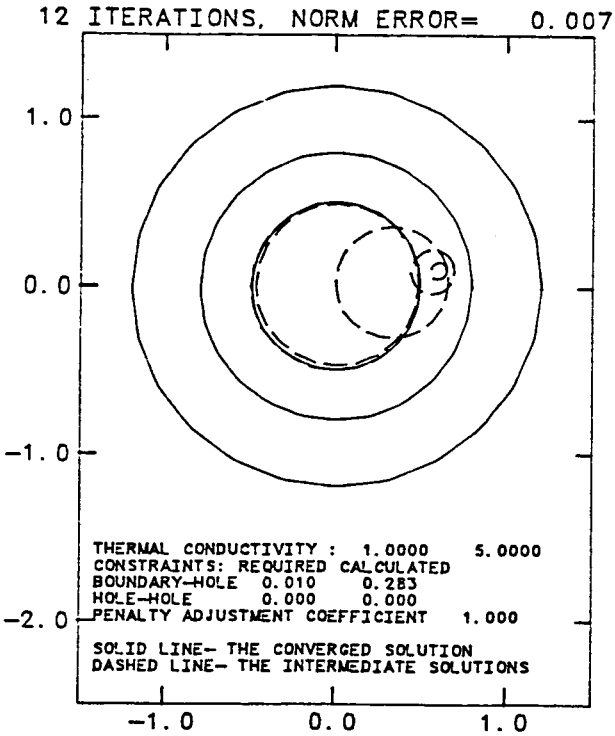

Fig. 4 Iteration sequence, test case 1

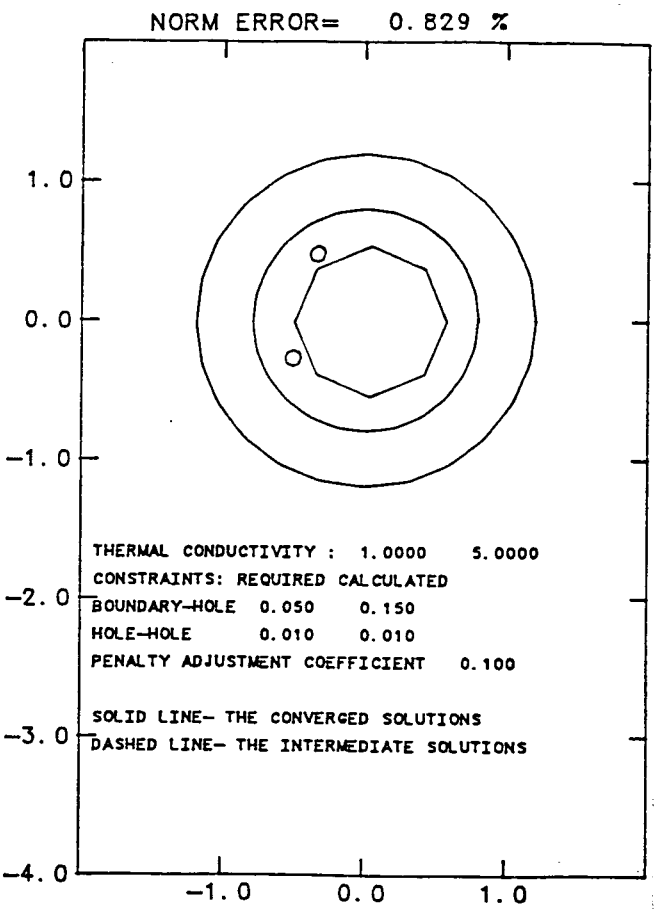

Fig. 5b Iteration sequence, test case 2

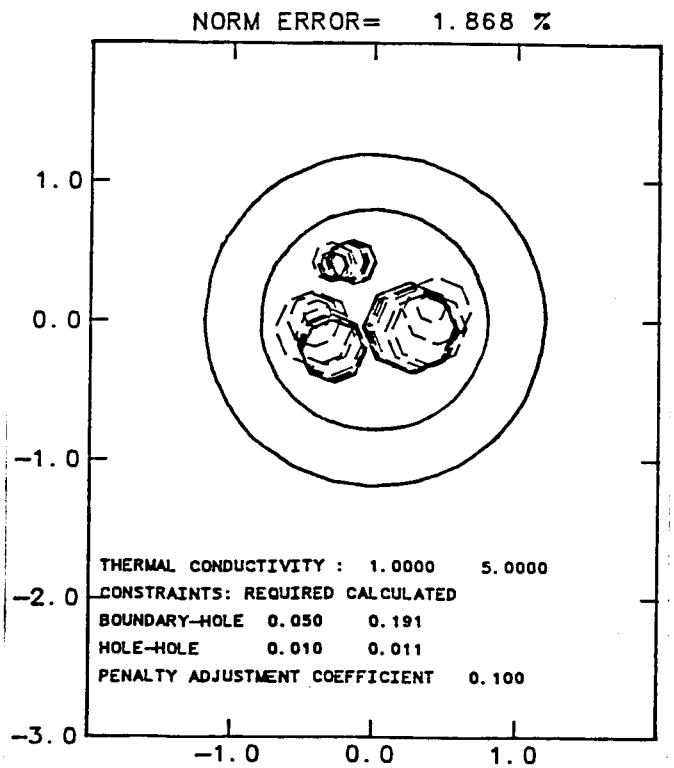

Fig. 5a Iteration sequence, test case 2

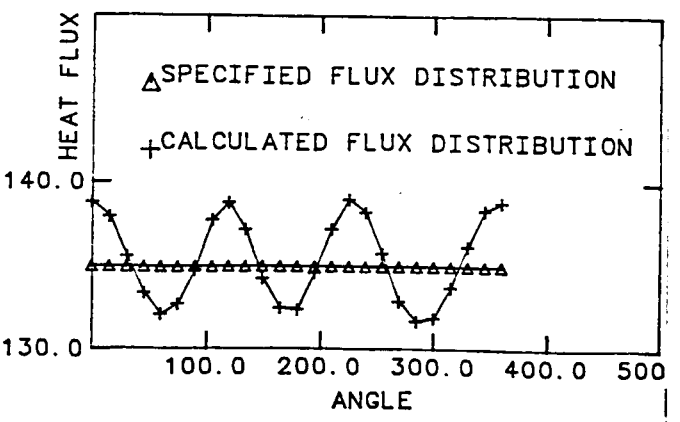

Fig. 6 Calaulated and specified heat flux distributions, test case 2

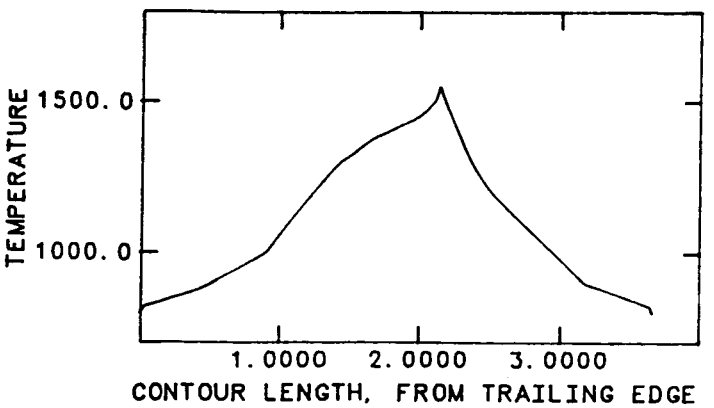

Fig. 7 Temperature distribution prescribed on Γ_1, test case 3

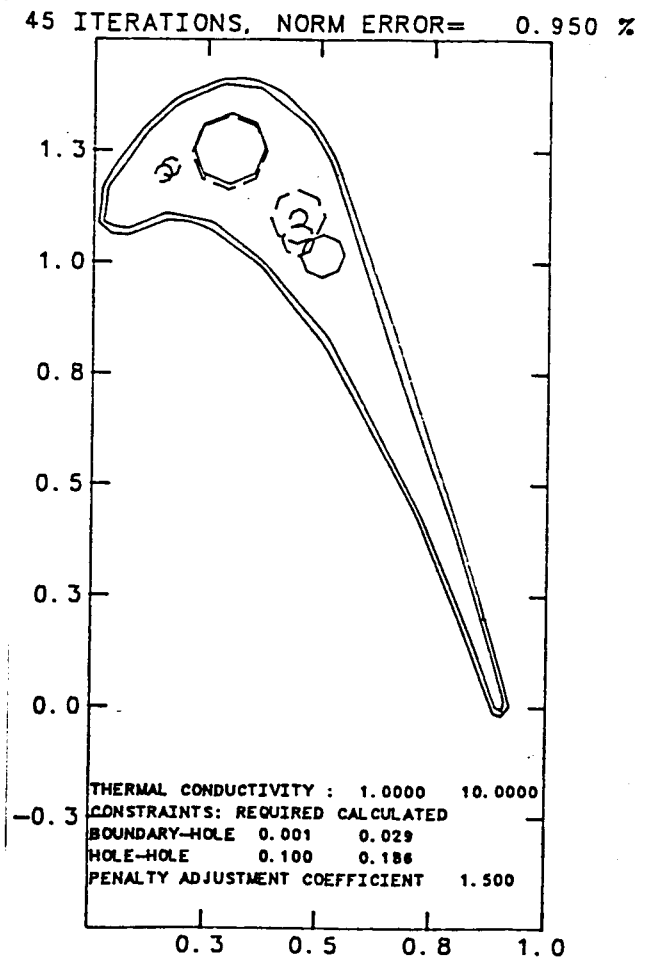

Fig. 8 Iteration sequence, test case 3

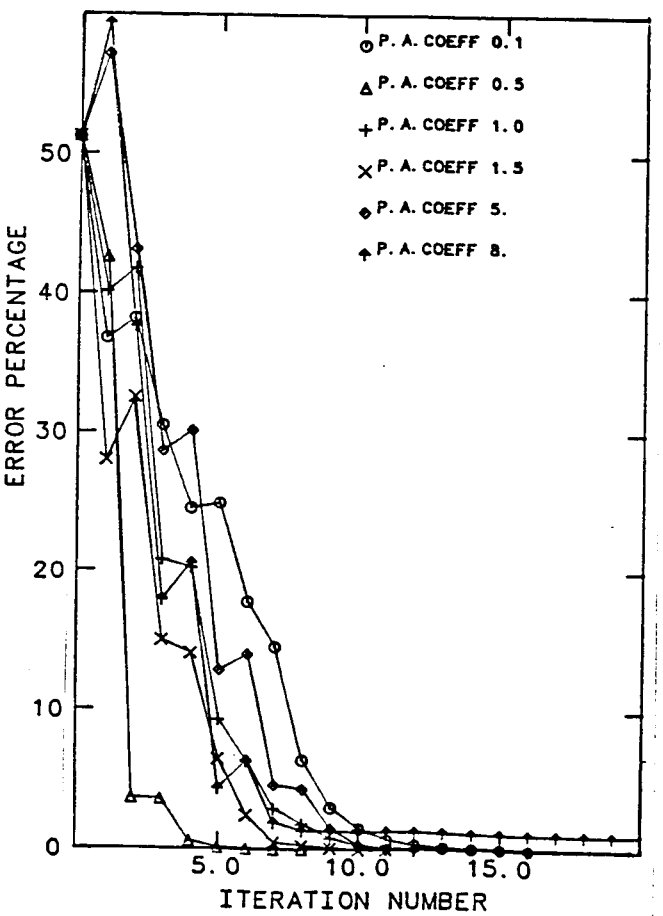

Fig. 9 Convergence history, test case 1

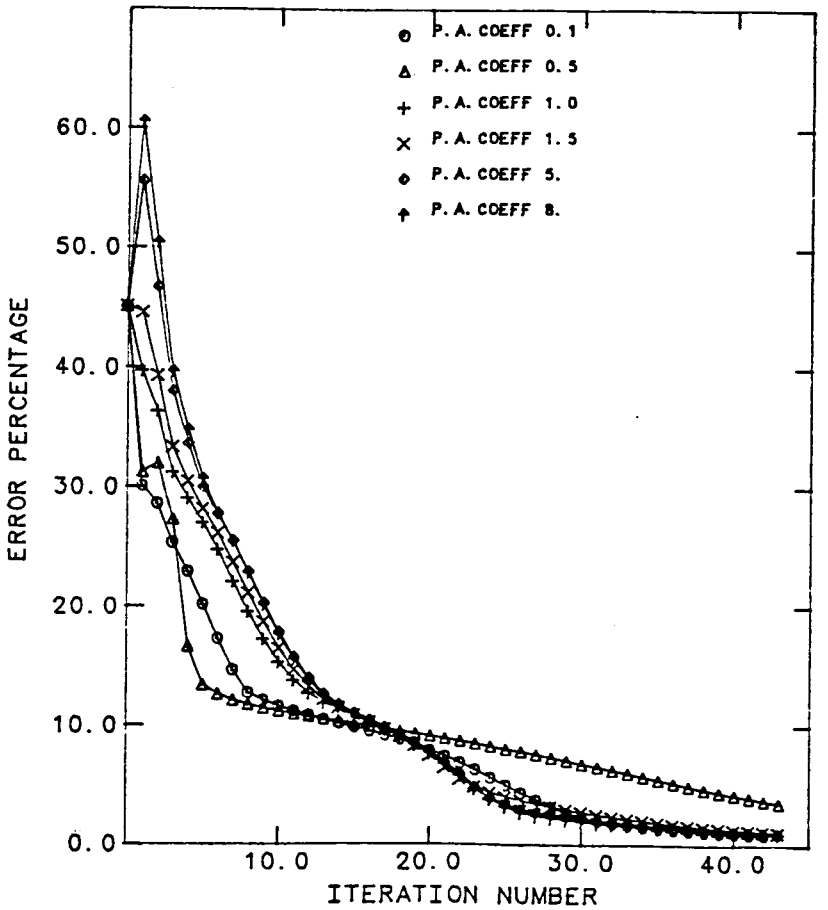

Fig. 10 Convergence history, test case 3